Supporting information for

High solar-to-hydrogen efficiency in the novel derivatives of group-III trichalcogenides for photocatalytic water splitting: the effect of elemental composition

Hao Ma[a], Wen Zhao[a,] *, Saifei Yuan[a], Hao Ren[a], Houyu Zhu[a], Yuhua Chi[a], Wenyue Guo[a,] *

[a] *School of Materials Science and Engineering, China University of Petroleum (East China), Qingdao 266580, Shandong, China*

* Corresponding author.

E-mail addresses: zhaowen@upc.edu.cn (Wen Zhao) and wyguo@upc.edu.cn (Wenyue Guo)

Table S1 Calculated lattice parameters (a=b), total heights (h), interlayer distances between the two Group-III metal layers (l), formation energies (E_{form}), band types, band gaps at the HSE level (E_g^{HSE}) and the PBE level (E_g^{PBE}), differences of electrostatic potential between the two surfaces ($\Delta\phi$), overpotentials for the hydrogen evolution reaction $\chi(H_2)$ and for the oxygen evolution reaction $\chi(O_2)$ of the MNX_3 (M, N = In/Ga/Al; X = S/Se/Te) monolayers, including α and β phases.

Materials MNX_3	$a = b$ (Å)	h (Å)	l (Å)	E_{form} (eV/atom)	Band type	E_g^{HSE} (eV)	E_g^{PBE} (eV)	$\Delta\phi$ (eV)	$\chi(H_2)$ (eV)	$\chi(O_2)$ (eV)
$InGaS_3$-α	3.81	6.09	3.86	-0.75	I	1.71	0.95	1.77	0.23	2.01
$InGaS_3$-β	3.77	6.25	3.91	-0.66	I	2.47	1.62	1.43	0.62	2.05
$InGaSe_3$-α	3.99	6.50	4.06	-0.74	I	1.07	0.43	1.42	0.02	1.23
$InGaSe_3$-β	3.95	6.64	4.10	-0.66	I	1.78	1.07	1.21	0.52	1.23
$InGaTe_3$-α	4.28	7.10	4.39	-0.47	I	0.68	0.17	1.02	0.28	0.19
$InGaTe_3$-β	4.26	7.23	4.44	-0.41	I	1.19	0.31	0.82	0.64	0.14
$InAlS_3$-α	3.79	6.06	3.86	-0.90	D	2.35	1.06	2.07	1.25	1.94
$InAlS_3$-β	3.72	6.25	3.89	-0.86	I	2.72	1.42	1.87	0.85	2.51
$InAlSe_3$-α	3.97	6.47	4.06	-0.83	D	1.67	0.58	1.58	0.81	1.21
$InAlSe_3$-β	3.91	6.62	4.07	-0.81	I	2.12	1.13	1.62	0.86	1.65
$InAlTe_3$-α	4.27	7.10	4.40	-0.49	I	1.18	0.41	1.13	0.88	0.21
$InAlTe_3$-β	4.24	7.19	4.38	-0.49	I	1.56	0.84	1.21	0.96	0.57
$GaAlS_3$-α	3.63	5.88	3.73	-0.93	I	2.62	1.62	1.87	1.33	1.92
$GaAlS_3$-β	3.61	5.89	3.71	-0.99	I	2.80	1.49	2.20	1.39	2.37
$GaAlSe_3$-α	3.83	6.30	3.94	-0.81	I	1.84	1.08	1.44	1.00	1.05
$GaAlSe_3$-β	3.81	6.28	3.90	-0.88	I	1.90	0.82	1.82	0.99	1.50
$GaAlTe_3$-α	4.15	6.92	4.30	-0.44	I	0.71	0.24	0.97	0.47	-0.02
$GaAlTe_3$-β	4.13	6.87	4.23	-0.51	I	1.24	0.48	1.30	0.92	0.39

Table S2 Calculated lattice parameters (a=b), total heights (h), interlayer distances between the two Group-III metal layers (l), formation energies (E_{form}), band types, band gaps at the HSE level (E_g^{HSE}) and the PBE level (E_g^{PBE}), differences of electrostatic potential between the two surfaces ($\Delta\phi$), overpotentials for the hydrogen evolution reaction $\chi(H_2)$ and the oxygen evolution reaction $\chi(O_2)$ of the $InGaXY_2$ (X, Y = S/Se/Te) monolayer, including α and β phases (here, the most stable configurations are highlighted with blue font, and a material with a bandgap below 0.4 eV is typically classified as a metal).

Materials	Type	$a=b$ (Å)	h (Å)	l (Å)	E_{form} (eV/atom)	Band type	E_g^{HSE} (eV)	E_g^{PBE} (eV)	$\Delta\phi$ (eV)	$\chi(H_2)$ (eV)	$\chi(O_2)$ (eV)
$InGaSSe_2$-α	I	3.92	6.43	4.09	-0.69	I	0.64	0.07	1.35	-0.29	1.05
	II	3.93	6.41	4.09	-0.71	I	1.47	0.72	1.74	0.27	1.71
	III	**3.95**	**6.32**	**3.84**	**-0.74**	**D**	**1.09**	**0.48**	**1.59**	**0.27**	**1.18**
$InGaSSe_2$-β	**I**	**3.89**	**6.55**	**4.12**	**-0.64**	**I**	**1.61**	**0.92**	**1.02**	**0.26**	**1.14**
	II	3.87	6.59	4.13	-0.61	I	1.84	1.07	1.50	0.50	1.61
	III	3.91	6.48	3.90	-0.63	I	2.13	1.41	1.30	0.72	1.48
$InGaSeS_2$-α	**I**	**3.89**	**6.21**	**3.86**	**-0.74**	**I**	**1.98**	**1.22**	**1.91**	**0.54**	**2.12**
	II	3.97	6.37	3.81	-0.52	M	-	-	0.61	-	-
	III	3.86	6.33	4.11	-0.69	I	1.15	0.40	1.64	-0.05	1.61
$InGaSeS_2$-β	I	3.82	6.41	3.91	-0.62	I	2.47	1.63	1.64	0.79	2.09
	II	**3.84**	**6.37**	**3.91**	**-0.64**	**I**	**1.93**	**1.22**	**1.15**	**0.48**	**1.36**
	III	3.82	6.48	4.14	-0.62	I	1.76	0.99	1.29	0.30	1.52
$InGaSTe_2$-α	I	4.11	6.91	4.47	-0.43	M	-	-	0.40	-	-
	II	4.13	6.85	4.44	-0.48	D	0.94	0.31	1.71	0.72	0.70
	III	**4.19**	**6.53**	**3.78**	**-0.55**	**D**	**0.94**	**0.42**	**1.21**	**0.78**	**0.14**
$InGaSTe_2$-β	**I**	**4.09**	**6.97**	**4.48**	**-0.44**	**M**	**0.38**	**0**	**0.45**	**-**	**-**
	II	4.09	7.04	4.47	-0.36	I	0.53	0	1.62	0.11	0.81
	III	4.16	6.69	3.86	-0.42	I	1.38	0.84	0.92	0.60	0.47
$InGaTeS_2$-α	**I**	**4.02**	**6.29**	**3.82**	**-0.63**	**I**	**2.52**	**1.82**	**2.03**	**1.27**	**2.04**
	II	3.97	6.36	3.81	-0.58	M	-	-	0.60	-	-
	III	3.94	6.69	4.58	-0.53	M	-	-	1.18	-	-
$InGaTeS_2$-β	I	3.95	6.53	3.88	-0.45	D	1.31	0.56	1.89	0.80	1.17
	II	**3.97**	**6.46**	**3.89**	**-0.52**	**D**	**0.67**	**0.13**	**0.68**	**0.22**	**-0.10**
	III	3.88	6.87	4.59	-0.48	M	-	-	0.93	-	-
$InGaSeTe_2$-α	I	4.17	7.00	4.44	-0.48	M	-	-	0.77	-	-
	II	4.21	6.94		-0.52	I	0.99	0.40	1.45	0.52	0.69
	III	**4.23**	**6.74**	**4.00**	**-0.55**	**D**	**0.86**	**0.36**	**1.16**	**0.56**	**0.23**
$InGaSeTe_2$-β	**I**	**4.15**	**7.09**	**4.46**	**-0.47**	**I**	**0.66**	**0.18**	**0.56**	**0.03**	**-0.04**
	II	4.13	7.15	4.45	-0.42	I	0.90	0.32	1.33	0.36	0.64
	III	4.21	6.89	4.07	-0.46	I	1.33	0.78	0.88	0.49	0.49
$InGaTeSe_2$-α	**I**	**4.12**	**6.60**	**4.03**	**-0.64**	**I**	**1.98**	**1.28**	**1.64**	**1.00**	**1.39**
	II	4.10	6.65	4.02	-0.60	M	-	-	1.01	-	-
	III	4.07	6.87	4.49	-0.57	M	-	-	1.16	-	-
$InGaTeSe_2$-β	I	4.08	6.80	4.08	-0.51	D	1.51	0.81	1.44	0.56	1.16
	II	**4.08**	**6.76**	**4.09**	**-0.56**	**I**	**1.10**	**0.57**	**0.69**	**0.34**	**0.22**
	III	4.03	7.0	4.48	-0.53	D	0.76	0.19	1.01	0.17	0.37

Table S3 Calculated lattice parameters (a=b), total heights (h), interlayer distances between the two Group-III metal layers (l), formation energies (E_{form}), band types, band gaps at the HSE level (E_g^{HSE}) and the PBE level (E_g^{PBE}), differences of electrostatic potential between the two surfaces ($\Delta\phi$), overpotentials for the hydrogen evolution reaction $\chi(H_2)$ and the oxygen evolution reaction $\chi(O_2)$ of the $InAlXY_2$ (X, Y = S/Se/Te) monolayers, including α and β phases (here, the most stable configurations are highlighted with blue font, and a material with a bandgap below 0.4 eV is typically classified as a metal).

Materials	Type	$a=b$ (Å)	h (Å)	l (Å)	E_{form} (eV/atom)	Band type	E_g^{HSE} (eV)	E_g^{PBE} (eV)	$\Delta\phi$ (eV)	$\chi(H_2)$ (eV)	$\chi(O_2)$ (eV)
$InAlSSe_2$-α	I	3.89	6.38	4.08	-0.84	D	1.27	0.61	1.71	0.75	0.99
	II	3.75	6.37	4.07	-0.82	I	2.14	1.31	1.86	1.03	1.73
	III	**3.78**	**6.26**	**3.82**	**-0.87**	**D**	**1.81**	**1.12**	**1.62**	**1.06**	**1.14**
$InAlSSe_2$-β	I	3.86	6.50	4.08	-0.82	I	1.88	1.18	1.46	0.52	1.58
	II	**3.73**	**6.54**	**4.09**	**-0.82**	**I**	**2.40**	**1.60**	**1.80**	**0.97**	**2.00**
	III	3.75	6.44	3.85	-0.82	I	2.18	1.52	1.86	1.04	1.77
$InAlSeS_2$-α	I	3.87	6.16	3.84	-0.87	I	2.73	1.92	1.92	1.32	2.10
	II	**3.70**	**6.17**	**3.84**	**-0.89**	**D**	**1.37**	**0.70**	**1.77**	**1.01**	**0.89**
	III	3.68	6.27	4.10	-0.84	I	1.82	1.01	1.99	0.97	1.61
$InAlSeS_2$-β	**I**	**3.78**	**6.36**	**3.87**	**-0.84**	**I**	**2.66**	**1.83**	**2.07**	**1.17**	**2.33**
	II	3.68	6.33	3.87	-0.83	D	1.86	1.21	1.70	0.72	1.62
	III	3.67	6.42	4.10	-0.83	I	2.23	1.41	1.60	0.65	1.94
$InAlSTe_2$-α	I	4.06	6.88	4.46	-0.53	M	-	-	1.18	-	-
	II	3.96	6.83	4.44	-0.53	D	1.27	0.56	1.75	1.06	0.74
	III	**4.06**	**6.49**	**3.75**	**-0.63**	**I**	**1.38**	**0.83**	**1.10**	**1.11**	**0.14**
$InAlSTe_2$-β	**I**	**4.07**	**6.92**	**4.42**	**-0.56**	**I**	**0.57**	**0.07**	**0.83**	**-0.07**	**0.25**
	II	3.94	7.00	4.42	-0.53	I	1.39	0.79	1.78	0.99	0.95
	III	4.00	6.68	3.81	-0.55	I	1.58	1.08	1.55	1.25	0.65
$InAlTeS_2$-α	I	4.01	6.26	3.80	-0.72	I	3.13	2.17	1.89	1.62	2.17
	II	**3.79**	**6.30**	**3.79**	**-0.73**	**M**	**-**	**-**	**1.37**	**-**	**-**
	III	3.74	6.63	4.54	-0.64	M	-	-	1.77	-	-
$InAlTeS_2$-β	I	3.89	6.50	3.85	-0.66	I	1.42	0.76	2.30	1.19	1.30
	II	**3.80**	**6.44**	**3.83**	**-0.67**	**M**	**0.30**	**0**	**1.35**	**-**	**-**
	III	3.76	6.72	4.47	-0.66	D	0.77	0.14	1.25	0.31	0.48
$InAlSeTe_2$-α	I	4.15	6.97	4.43	-0.56	M	0.15	-	1.06	-	-
	II	4.04	6.95	4.43	-0.56	I	1.46	0.79	1.53	1.09	0.66
	III	**4.08**	**6.72**	**3.99**	**-0.62**	**I**	**1.36**	**0.83**	**1.15**	**1.08**	**0.20**
$InAlSeTe_2$-β	**I**	**4.14**	**7.02**	**4.40**	**-0.58**	**I**	**0.89**	**0.36**	**0.96**	**0.21**	**0.41**
	II	4.02	7.08	4.41	-0.56	I	1.67	1.07	1.61	1.00	1.05
	III	4.07	6.87	4.02	-0.58	I	1.69	1.18	1.40	1.14	0.72
$InAlTeSe_2$-α	**I**	**4.12**	**6.57**	**4.02**	**-0.71**	**I**	**2.43**	**1.66**	**1.60**	**1.38**	**1.43**
	II	3.95	6.61	4.02	-0.71	M	0.19	0	1.19	-	-
	III	3.89	6.83	4.48	-0.66	D	0.51	0	1.44	0.40	0.32
$InAlTeSe_2$-β	I	4.02	6.77	4.04	-0.67	I	1.92	1.24	1.86	1.14	1.40
	II	**3.93**	**6.73**	**4.04**	**-0.69**	**D**	**0.96**	**0.46**	**1.21**	**0.55**	**0.40**
	III	3.90	6.93	4.44	-0.68	D	1.24	0.61	1.32	0.53	0.80

Table S4 Calculated lattice parameters (a=b), total heights (h), interlayer distances between the two Group-III metal layers (l), formation energies (E_{form}), band types, band gaps at the HSE level (E_g^{HSE}) and the PBE level (E_g^{PBE}), differences of electrostatic potential between the two surfaces ($\Delta\phi$), overpotentials for the hydrogen evolution reaction $\chi(H_2)$ and the oxygen evolution reaction $\chi(O_2)$ of the $GaAlXY_2$ (X, Y = S/Se/Te) monolayers, including α and β phases (here, the most stable configurations are highlighted with blue font, and a material with a bandgap below 0.4 eV is typically classified as a metal).

Materials	Type	$a=b$ (Å)	h (Å)	l (Å)	E_{form} (eV/atom)	Band type	E_g^{HSE} (eV)	E_g^{PBE} (eV)	$\Delta\phi$ (eV)	$\chi(H_2)$ (eV)	$\chi(O_2)$ (eV)
$GaAlSSe_2$-α	I	3.75	6.18	3.95	-0.85	I	1.66	0.96	1.53	1.07	0.89
	II	3.92	6.21	3.96	-0.81	I	2.01	1.23	1.76	1.14	1.40
	III	**3.93**	**6.09**	**3.71**	**-0.86**	**I**	**2.10**	**1.40**	**1.45**	**1.12**	**1.21**
$GaAlSSe_2$-β	**I**	**3.74**	**6.19**	**3.92**	**-0.91**	**I**	**1.52**	**0.82**	**1.70**	**0.64**	**1.36**
	II	3.83	6.19	3.93	-0.91	I	2.42	1.58	2.02	1.35	1.85
	III	3.86	6.09	3.68	-0.88	D	1.99	1.30	2.06	1.32	1.51
$GaAlSeS_2$-α	I	3.71	6.00	3.72	-0.86	I	2.74	1.88	1.79	1.28	2.02
	II	**3.84**	**5.97**	**3.72**	**-0.90**	**I**	**1.84**	**1.16**	**1.55**	**1.20**	**0.97**
	III	3.83	6.09	3.97	-0.86	I	1.81	1.04	1.81	1.17	1.22
$GaAlSeS_2$-β	**I**	**3.68**	**6.00**	**3.70**	**-0.95**	**I**	**3.01**	**2.17**	**2.30**	**1.65**	**2.43**
	II	3.80	5.99	3.69	-0.93	D	1.53	0.85	1.99	1.00	1.28
	III	3.78	6.08	3.94	-0.93	I	2.08	1.24	1.90	1.00	1.74
$GaAlSTe_2$-α	I	3.93	6.70	4.35	-0.54	M	0.12	0	1.03	-	-
	II	4.14	6.73	4.34	-0.45	D	0.69	0.13	1.79	0.83	0.42
	III	**4.19**	**6.32**	**3.66**	**-0.58**	**I**	**1.13**	**0.60**	**0.85**	**0.57**	**0.17**
$GaAlSTe_2$-β	I	3.95	6.64	4.28	-0.55	M	-	-	1.00	-	-
	II	4.02	6.64	4.28	-0.59	I	1.17	0.61	1.91	1.13	0.71
	III	**4.12**	**6.35**	**3.64**	**-0.62**	**I**	**1.11**	**0.66**	**1.67**	**1.24**	**0.32**
$GaAlTeS_2$-α	I	3.85	6.14	3.70	-0.65	I	2.19	1.39	1.82	1.24	1.54
	II	**3.95**	**6.14**	**3.67**	**-0.74**	**M**	**-**	**-**	**1.20**	**-**	**-**
	III	3.92	6.53	4.47	-0.65	M	-	-	1.48	-	-
$GaAlTeS_2$-β	**I**	**3.80**	**6.12**	**3.67**	**-0.77**	**I**	**1.85**	**1.17**	**2.44**	**1.40**	**1.66**
	II	3.93	6.12	3.64	-0.73	M	-	-	1.46	-	-
	III	3.87	6.40	4.34	-0.71	M	0.19	0	1.46	-	-
$GaAlSeTe_2$-α	I	4.01	6.80	4.32	-0.54	I	0.42	-	0.88	0.43	-0.36
	II	4.19	6.81	4.32	-0.50	I	0.86	0.31	1.47	0.72	0.37
	III	**4.22**	**6.55**	**3.90**	**-0.57**	**I**	**1.15**	**0.63**	**0.95**	**0.63**	**0.24**
$GaAlSeTe_2$-β	I	4.02	6.74	4.25	-0.58	M	0.24	0	1.05	-	-
	II	4.12	6.74	4.26	-0.60	I	1.40	0.83	1.72	1.07	0.82
	III	**4.16**	**6.53**	**3.86**	**-0.63**	**I**	**1.29**	**0.83**	**1.50**	**1.08**	**0.48**
$GaAlTeSe_2$-α	I	3.97	6.44	3.92	-0.65	I	1.97	1.26	1.50	1.00	1.24
	II	**4.08**	**6.41**	**3.67**	**-0.69**	**I**	**0.74**	**0.24**	**0.93**	**0.65**	**-0.20**
	III	4.05	6.70	4.38	-0.64	M	0.40	0	1.27	-	-
$GaAlTeSe_2$-β	**I**	**3.94**	**6.41**	**3.88**	**-0.74**	**I**	**2.11**	**1.48**	**2.00**	**1.24**	**1.64**
	II	4.04	6.42	3.87	-0.72	M	0.23	0	1.39	-	-
	III	4.00	6.61	4.29	-0.71	D	0.73	0.12	1.44	0.45	0.48

Table S5 The efficiency of light absorption (η_{abs}), the efficiency of carrier utilization (η_{cu}), the STH efficiency (η_{STH}), and the corrected STH efficiency (η'_{STH}) of the MNX_3 (M, N = In/Ga/Al; X = S/Se/Te) monolayers, including α and β phases.

Materials MNX_3	η_{abs}(%)	η_{cu}(%)	η_{STH}(%)	η'_{STH}(%)
$InGaS_3$-α	50.5	53.8	27.2	19.6
$InGaS_3$-β	18.7	42.8	8.01	7.3
$InGaSe_3$-α	81.9	56.4	46.2	28.3
$InGaSe_3$-β	47.1	52.7	24.9	20.0
$InGaTe_3$-α	96.0	56.9	54.7	33.7
$InGaTe_3$-β	76.7	38.5	29.5	22.2
$InAlS_3$-α	22.5	44.2	9.95	8.53
$InAlS_3$-β	11.7	40.0	4.69	4.37
$InAlSe_3$-α	52.8	54.7	28.9	21.1
$InAlSe_3$-β	31.3	47.2	14.8	12.4
$InAlTe_3$-α	77.4	41.8	32.4	22.1
$InAlTe_3$-β	58.2	56.7	33.0	24.9
$GaAlS_3$-α	14.4	41.2	5.91	5.42
$GaAlS_3$-β	9.8	39.1	3.82	3.61
$GaAlSe_3$-α	43.9	51.5	22.6	17.9
$GaAlSe_3$-β	41.0	50.5	20.7	15.9
$GaAlTe_3$-α	-	-	-	-
$GaAlTe_3$-β	73.8	51.1	37.8	25.3

Table S6 The efficiency of light absorption (η_{abs}), the efficiency of carrier utilization (η_{cu}), the STH efficiency (η_{STH}), and the corrected STH efficiency (η'_{STH}) of the most stable $InGaXY_2$ (X, Y = S/Se/Te) monolayers, including α and β phases.

Materials	Type	η_{abs}(%)	η_{cu}(%)	η_{STH}(%)	η'_{STH}(%)
$InGaSSe_2$-α	III	81.3	67.0	54.5	32.0
$InGaSSe_2$-β	I	55.2	55.6	30.7	24.5
$InGaSeS_2$-α	I	37.3	49.2	18.4	14.3
$InGaSeS_2$-β	II	40.0	50.2	20.1	16.9
$InGaSTe_2$-α	III	88.6	45.9	40.6	25.0
$InGaSTe_2$-β	I	-	-	-	-
$InGaTeS_2$-α	I	17.3	42.3	7.3	6.5
$InGaTeS_2$-β	II	-	-	-	-
$InGaSeTe_2$-α	III	89.1	52.7	47.0	29.3
$InGaSeTe_2$-β	I	-	-	-	-
$InGaTeSe_2$-α	I	37.4	49.3	18.5	14.8
$InGaTeSe_2$-β	II	81.2	44.8	36.4	27.9

Table S7 The efficiency of light absorption (η_{abs}), the efficiency of carrier utilization (η_{cu}), the STH efficiency (η_{STH}), and the corrected STH efficiency (η'_{STH}) of the most stable $InAlXY_2$ (X, Y = S/Se/Te) monolayers, including α and β phases.

Materials	Type	η_{abs}(%)	η_{cu}(%)	η_{STH}(%)	η'_{STH}(%)
$InAlSSe_2$-α	III	45.4	52.1	23.7	18.0
$InAlSSe_2$-β	II	20.9	43.6	9.1	8.0
$InAlSeS_2$-α	II	68.6	60.8	41.7	26.1
$InAlSeS_2$-β	I	13.3	40.7	5.4	5.0
$InAlSTe_2$-α	III	68.1	33.2	22.6	16.5
$InAlSTe_2$-β	I	-	-	-	-
$InAlTeS_2$-α	II	-	-	-	-
$InAlTeS_2$-β	II	-	-	-	-
$InAlSeTe_2$-α	III	69.3	37.0	25.7	18.4
$InAlSeTe_2$-β	I	89.1	61.6	54.8	36.6
$InAlTeSe_2$-α	I	19.9	43.3	8.6	7.8
$InAlTeSe_2$-β	II	87.4	58.6	51.3	31.8

Table S8 The efficiency of light absorption (η_{abs}), the efficiency of carrier utilization (η_{cu}), the STH efficiency (η_{STH}), and the corrected STH efficiency (η'_{STH}) of the most stable $GaAlXY_2$ (X, Y = S/Se/Te) monolayers, including α and β phases.

Materials	Type	η_{abs}(%)	η_{cu}(%)	η_{STH}(%)	η'_{STH}(%)
$GaAlSSe_2$-α	III	32.1	47.5	15.2	12.9
$GaAlSSe_2$-β	I	60..3	57.5	34.7	23.4
$GaAlSeS_2$-α	II	43.9	51.5	22.6	17.6
$GaAlSeS_2$-β	I	5.9	37.0	2.2	2.1
$GaAlSTe_2$-α	III	80.0	41.2	33.0	24.2
$GaAlSTe_2$-β	III	81.0	49.9	40.4	23.3
$GaAlTeS_2$-α	II	-	-	-	
$GaAlTeS_2$-β	I	43.6	51.4	22.4	15.3
$GaAlSeTe_2$-α	III	79.1	44.4	35.1	25.0
$GaAlSeTe_2$-β	III	71.3	55.7	39.7	25.8
$GaAlTeSe_2$-α	II	-	-	-	-
$GaAlTeSe_2$-β	I	31.6	47.3	15.0	12.0

Table S9 The efficiency of light absorption (η_{abs}), the efficiency of carrier utilization (η_{cu}), the STH efficiency (η_{STH}), and the corrected STH efficiency (η'_{STH}) of the pristine Group-III metal trichalcogenide M_2X_3 monolayers (M = In/Ga/Al, X = S/Se/Te).

Materials MNX_3	η_{abs}(%)	η_{cu}(%)	η_{STH}(%)	η'_{STH}(%)
In_2S_3	37.7	49.4	18.6	14.8/14.4[1]
In_2Se_3	64.6	58.7	37.9	26.4/26.9[1]
In_2Te_3	77.1	53.0	40.9	28.9/32.1[1]
Ga_2S_3	15.1	41.5	6.3	5.8/6.4[1]
Ga_2Se_3	51.4	54.2	27.8	21.5/21.9[1]
Ga_2Te_3	-	-	-	-
Al_2S_3	7.9	38.2	3.0	2.9/2.6[1]
Al_2Se_3	21.6	43.9	9.5	8.2/8.0[1]
Al_2Te_3	62.9	45.7	28.7	20.1/21.4[1]

Table S10 Calculated lattice parameters (a=b), total heights (h), interlayer distances between the two Group-III metal layers (l), formation energies (E_{form}), band types, band gaps at the HSE level (E_g^{HSE}) and the PBE level (E_g^{PBE}), differences of electrostatic potential between the two surfaces ($\Delta\phi$), overpotentials for the hydrogen evolution reaction $\chi(H_2)$ and the oxygen evolution reaction $\chi(O_2)$ of the pristine Group-III trichalcogenide M_2X_3 monolayers (M = In/Ga/Al, X = S/Se/Te), as well as some available results[1,2].

Materials MNX_3	$a = b$ (Å)	h (Å)	l (Å)	E_{form} (eV/atom)	Band type	E_g^{HSE} (eV)	E_g^{PBE} (eV)	$\Delta\phi$ (eV)	$\chi(H_2)$ (eV)	$\chi(O_2)$ (eV)
In_2S_3	3.94	6.34	4.02	-0.68	In	1.97/1.91[1]/1.94[2]	1.20	1.69/1.68[1]/1.68[2]	0.26/0.21[1]/0.16[2]	2.18/2.15[1]/2.10[2]
In_2Se_3	4.11	6.79	4.22	-0.70	In	1.44/1.43[1]/1.37[2]	0.79	1.40/1.38[1]/1.22[2]	0.19/0.19[1]/0.13[2]	1.42/1.39[1]/1.40[2]
In_2Te_3	4.40	7.35	4.53	-0.46	In	1.19/1.14[1]/1.12[2]	0.64	1.01/1.00[1]/1.05[2]	0.57/0.50[1]/0.58[2]	0.39/0.41[1]/0.37[2]
Ga_2S_3	3.65	5.92	3.75	-0.79	In	2.59/2.55[1]/2.56[2]	1.69	1.63/1.65[1]/1.64[2]	1.06/1.05[1]/1.01[2]	1.93/1.92[1]/1.89[2]
Ga_2Se_3	3.84	6.33	3.94	-0.74	In	1.69/1.68[1]/1.64[2]	0.97	1.30/1.30[1]/1.30[2]	0.71/0.69[1]/0.65[2]	1.05/1.06[1] /1.06[2]
Ga_2Te_3	4.15	6.93	4.28	-0.44	In	0.74/0.77[1]/0.72[2]	0.25	0.88/0.88[1]/0.88[2]	0.43/0.43[1]/0.36[2]	-0.05/-0.01[1]/0.01[2]
Al_2S_3	3.59	5.82	3.69	-1.17	In	2.90/2.94[1]	2.12	2.42/2.35[1]	1.73/1.72[1]	2.35/2.34[1]
Al_2Se_3	3.79	6.24	3.90	-0.99	In	2.38/2.41[1]	1.70	1.98/1.96[1]	1.64/1.63[1]	1.50/1.51[1]
Al_2Te_3	4.12	6.87	4.24	-0.55	In	1.47/1.51[1]	0.93	1.44/1.43[1]	1.28/1.27[1]	0.40/0.43[1]

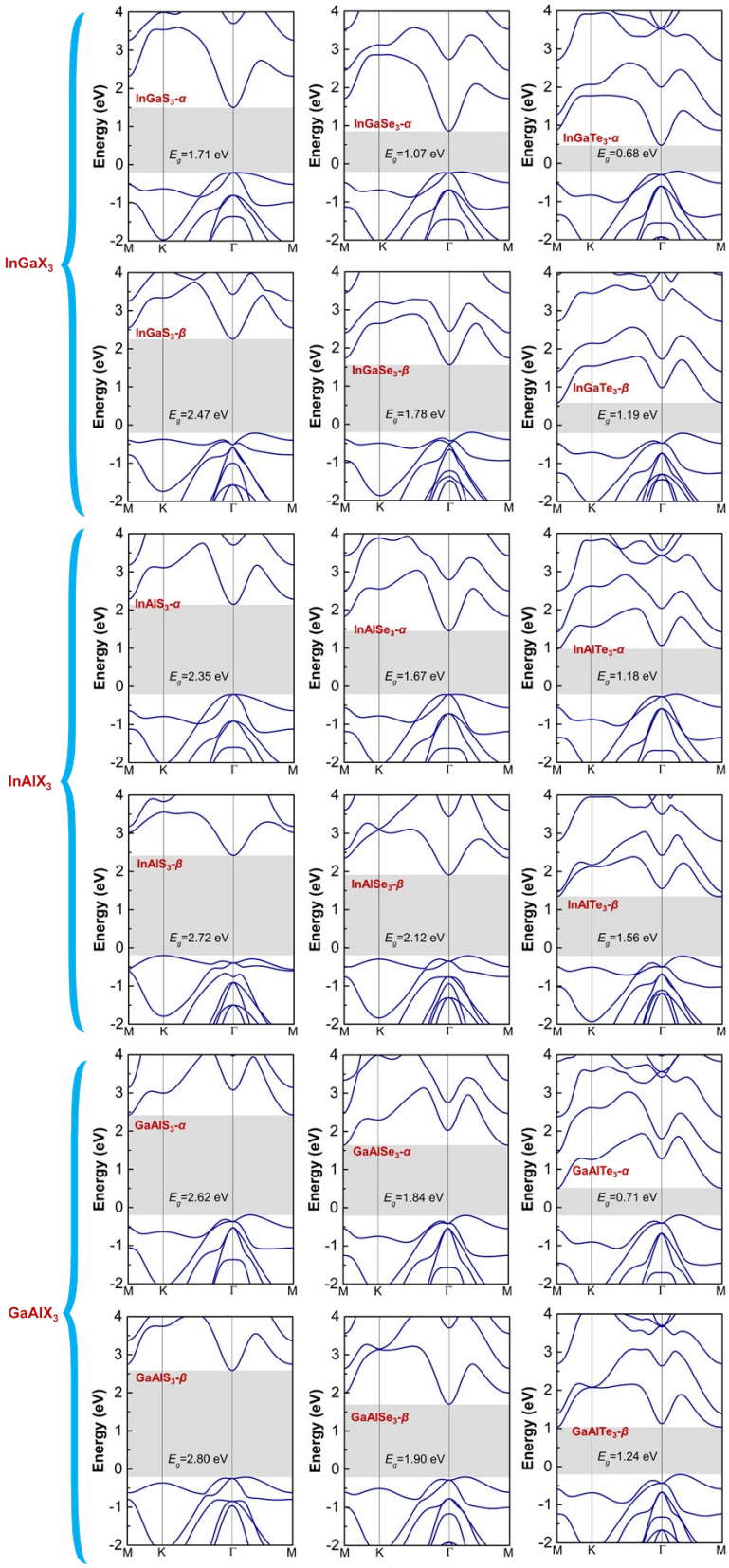

Figure S1 Calculated band structures of the MNX_3 (M, N = In/Ga/Al; X = S/Se/Te) monolayers under the HSE functional, including α and β phases. The Fermi levels are set to 0 eV.

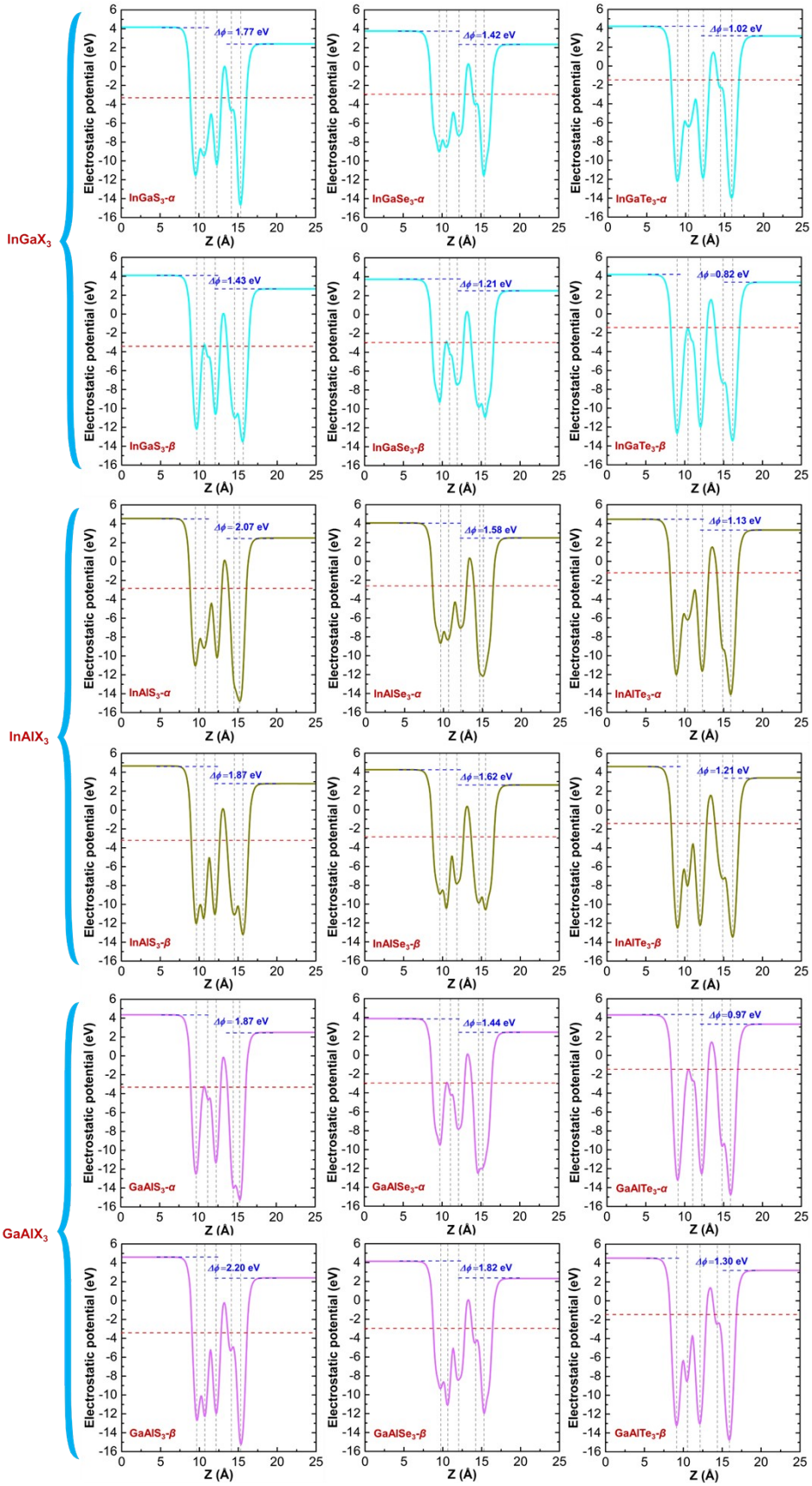

Figure S2 Calculated plane-averaged electrostatic differences of the MNX_3 (M, N = In/Ga/Al; X = S/Se/Te) monolayers, including α and β phases.

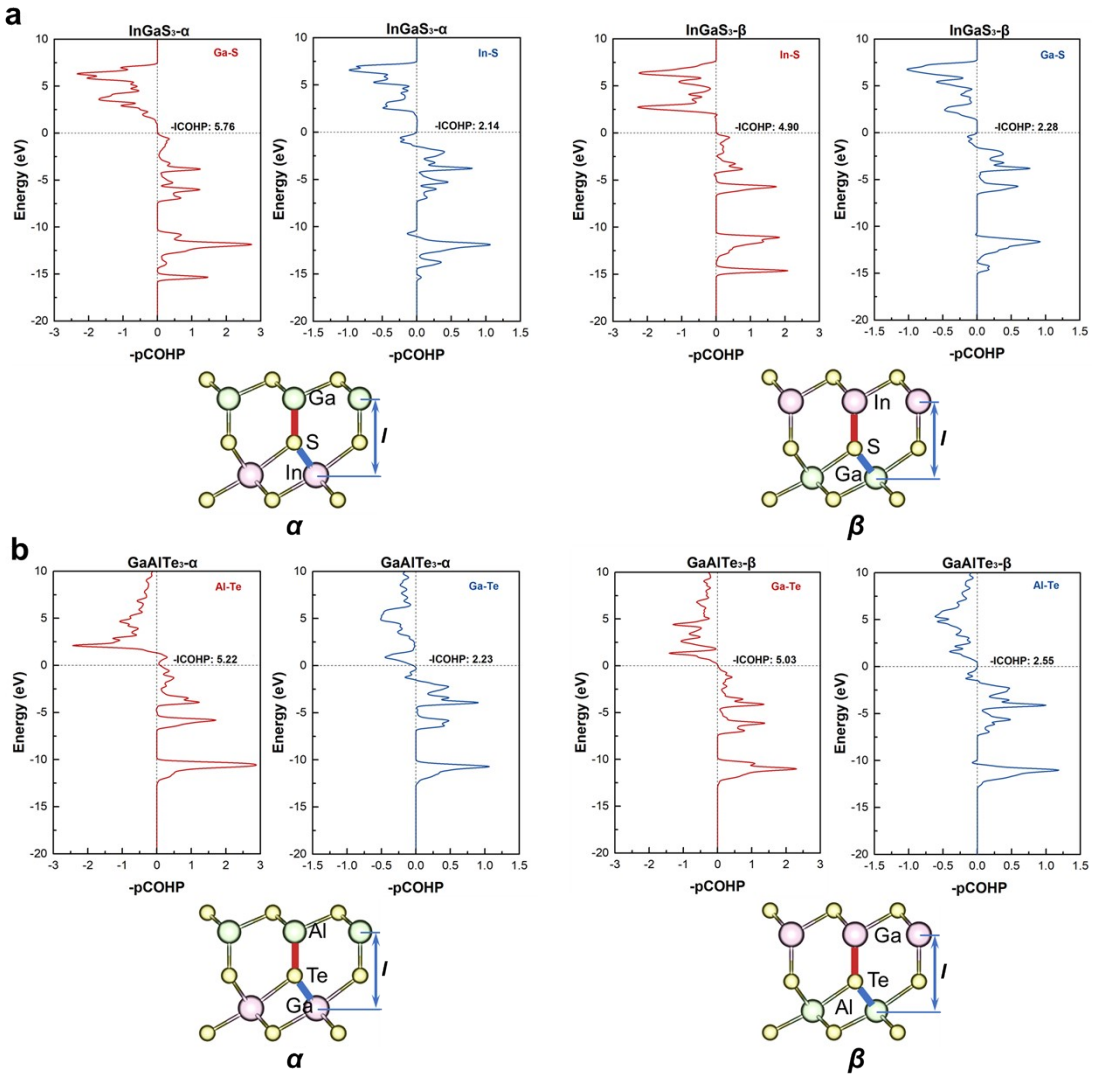

Figure S3 Chemical-bonding analysis of the middle-layer chalcogenides with adjacent metals in $InGaS_3$-*α*/*β* and $GaAlTe_3$-*α*/*β* with bonding levels to the right and antibonding ones to the left. The colors of the COHP plot correspond to the bonds highlighted in the structural fragments shown.

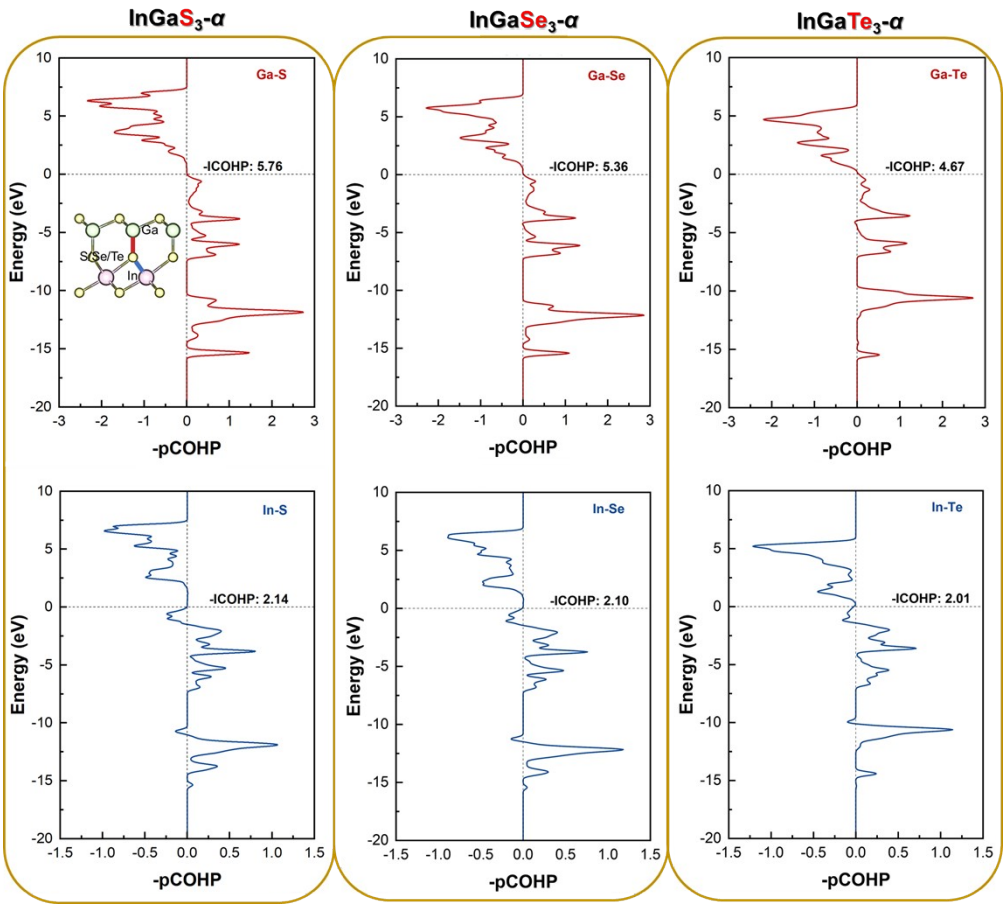

Figure S4 Chemical-bonding analysis of the middle-layer chalcogenides with adjacent metals in $InGaS_3$-α, $InGaSe_3$-α, and $InGaTe_3$-α with bonding levels to the right and antibonding ones to the left. The colors of the COHP plot correspond to the bonds highlighted in the structural fragments shown in the upper left corner.

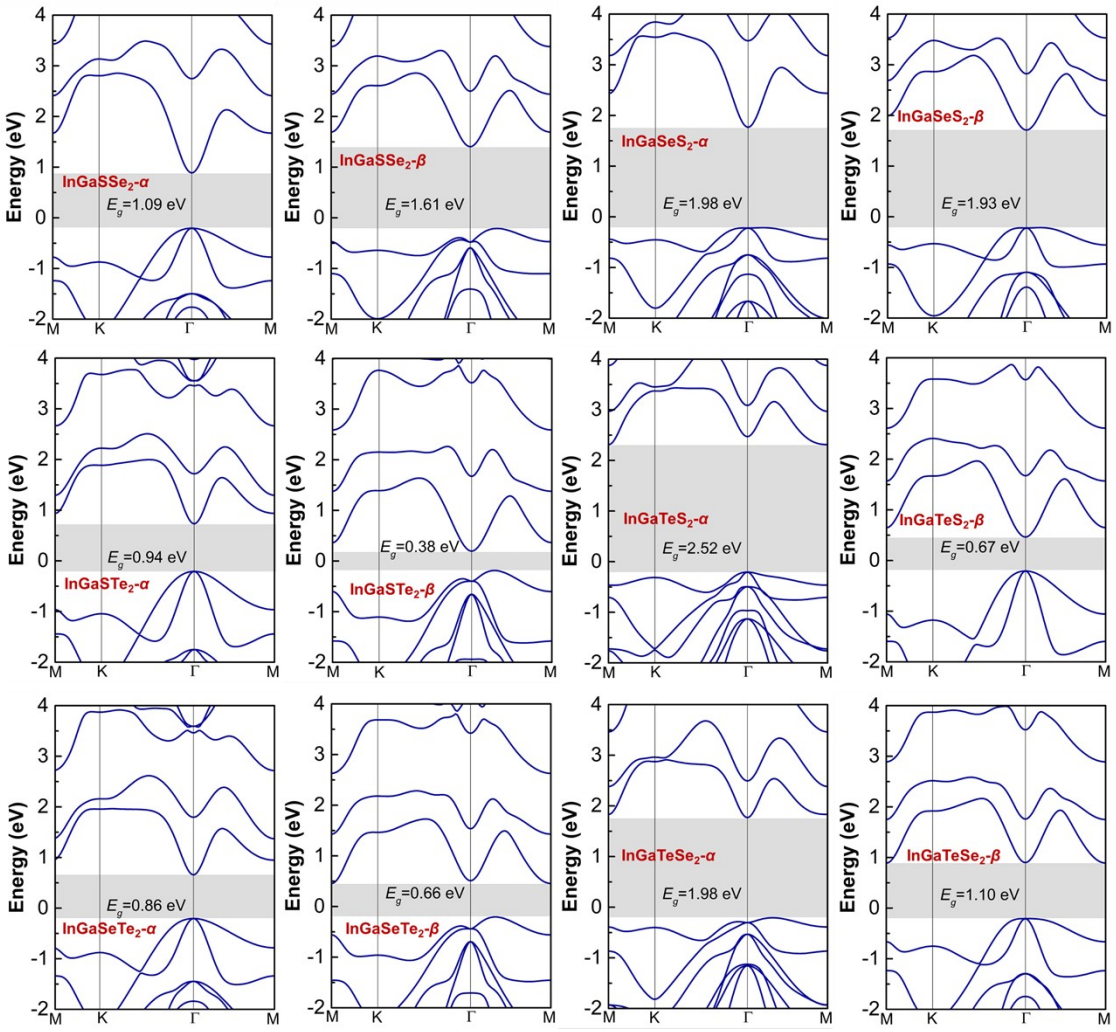

Figure S5 Calculated band structures of the most stable $InGaXY_2$ (X, Y=S/Se/Te) monolayers under the HSE functional, including α and β phases. The Fermi levels are set to 0 eV.

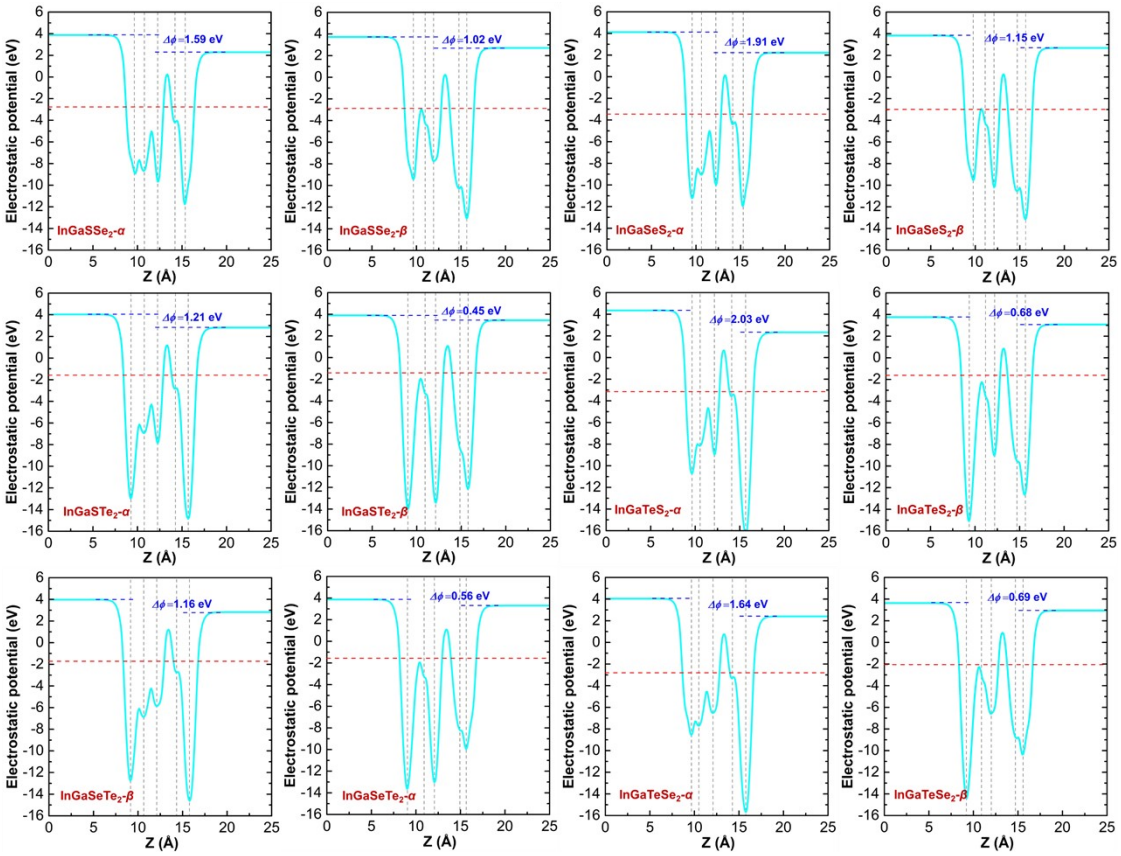

Figure S6 Calculated plane-averaged electrostatic differences of the most stable $InGaXY_2$ (X, Y=S/Se/Te) monolayers, including α and β phases.

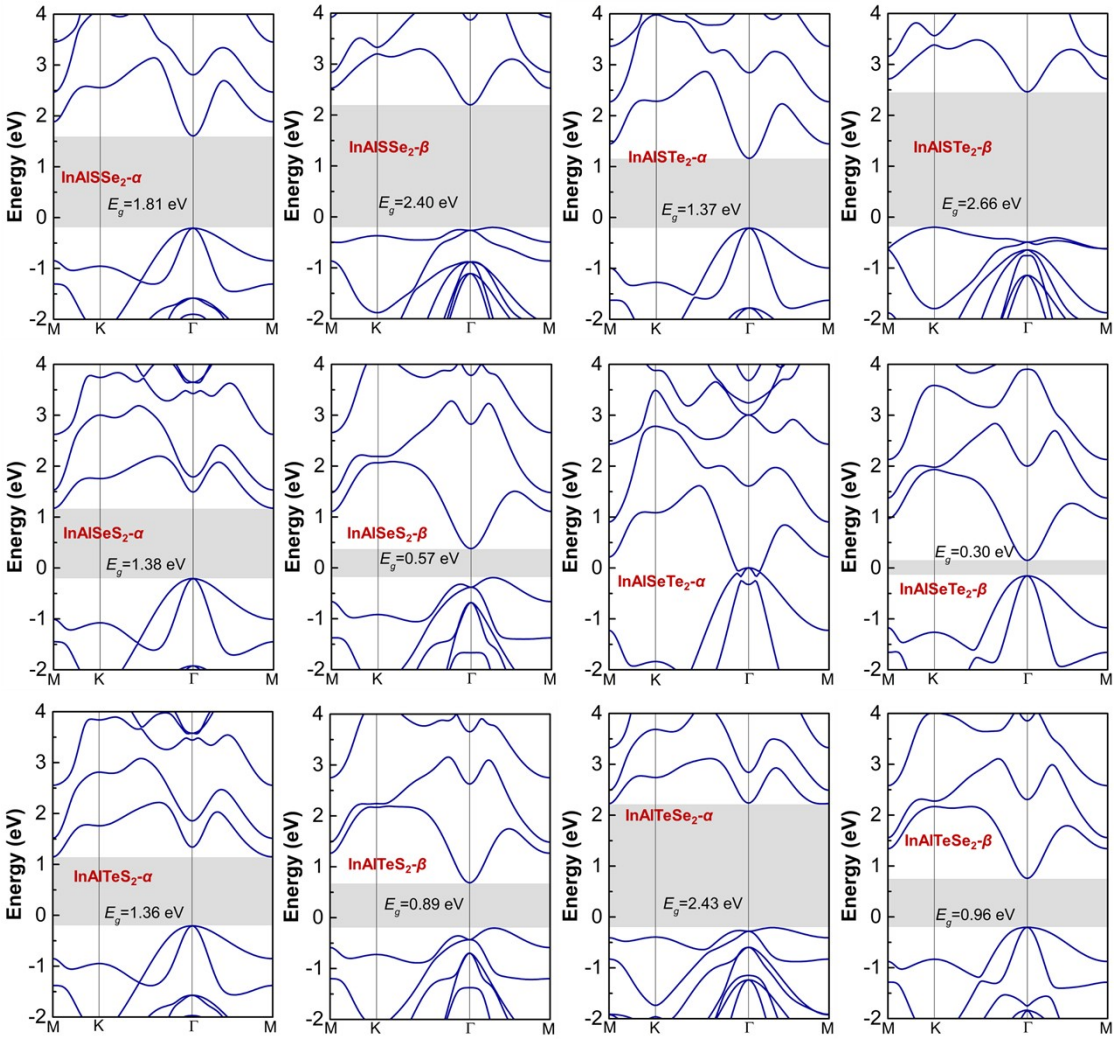

Figure S7 Calculated band structures of the most stable $InAlXY_2$ (X, Y = S/Se/Te) monolayers under the HSE functional, including α and β phases. The Fermi levels are set to 0 eV.

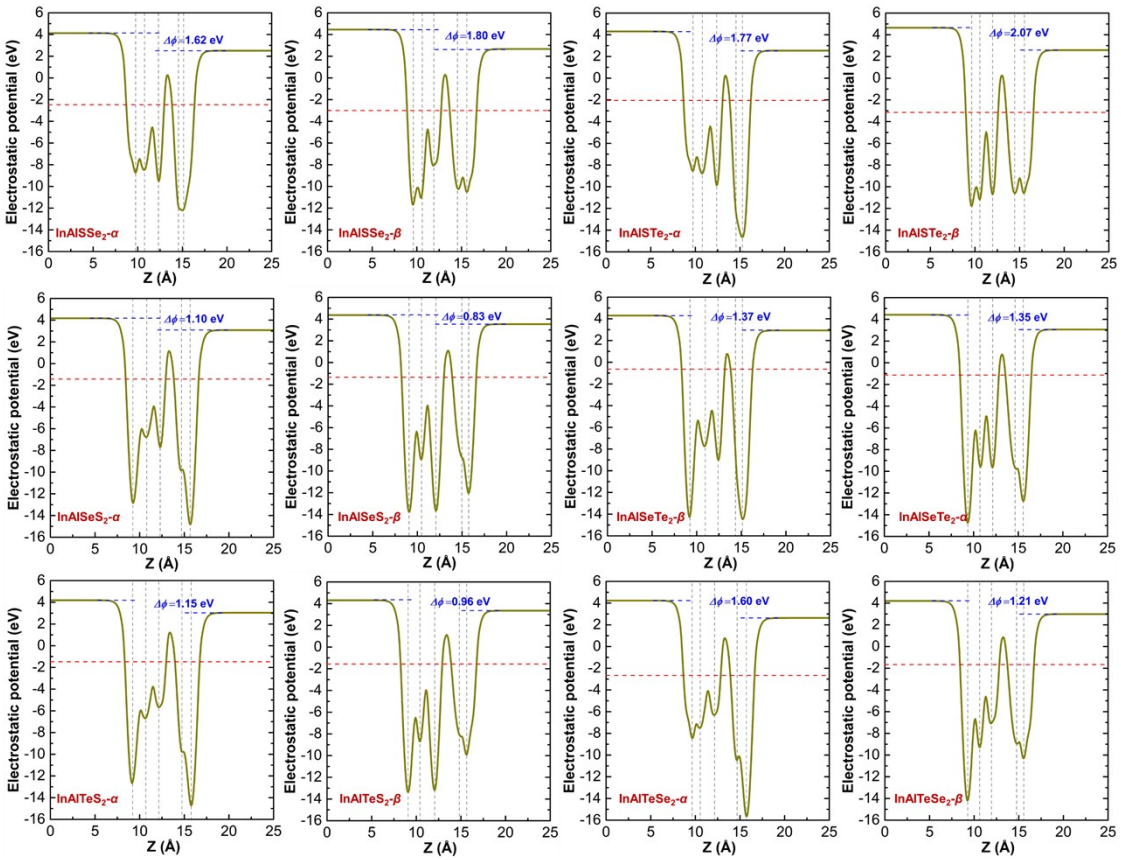

Figure S8 Calculated plane-averaged electrostatic differences of the most stable $InAlXY_2$ (X, Y = S/Se/Te) monolayers, including α and β phases.

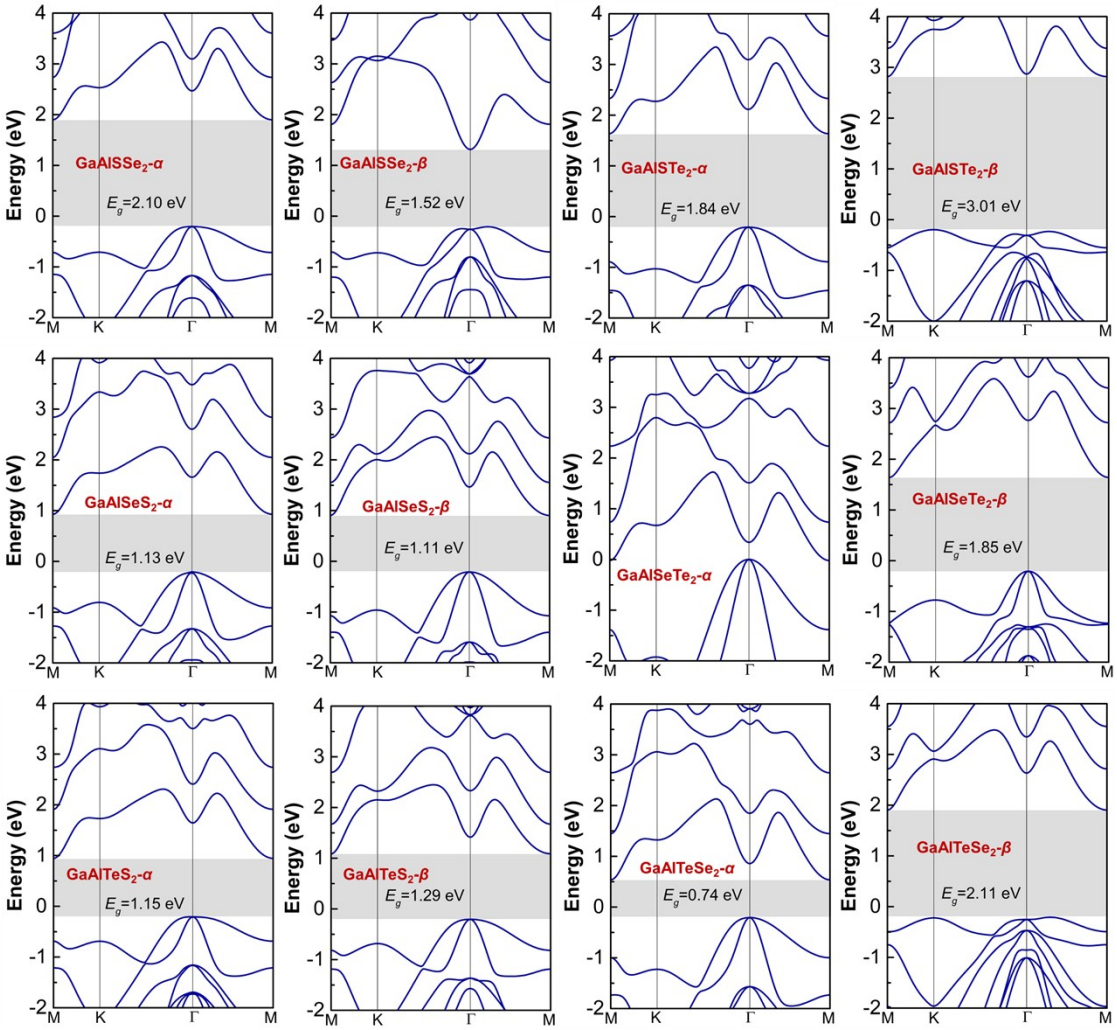

Figure S9 Calculated band structures of the most stable $GaAlXY_2$ (X, Y=S/Se/Te) monolayers under the HSE functional, including α and β phases. The Fermi levels are set to 0 eV.

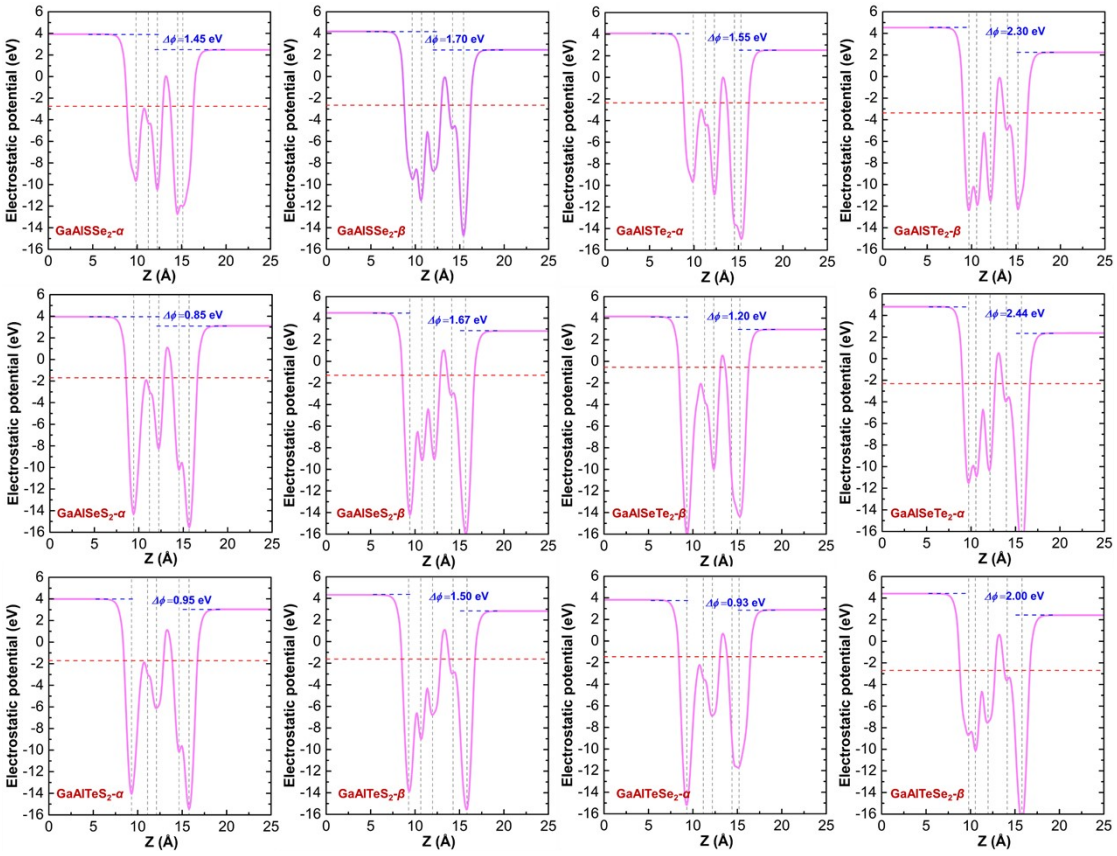

Figure S10 Calculated plane-averaged electrostatic differences of the most stable $GaAlXY_2$ (X, Y = S/Se/Te) monolayers, including α and β phases.

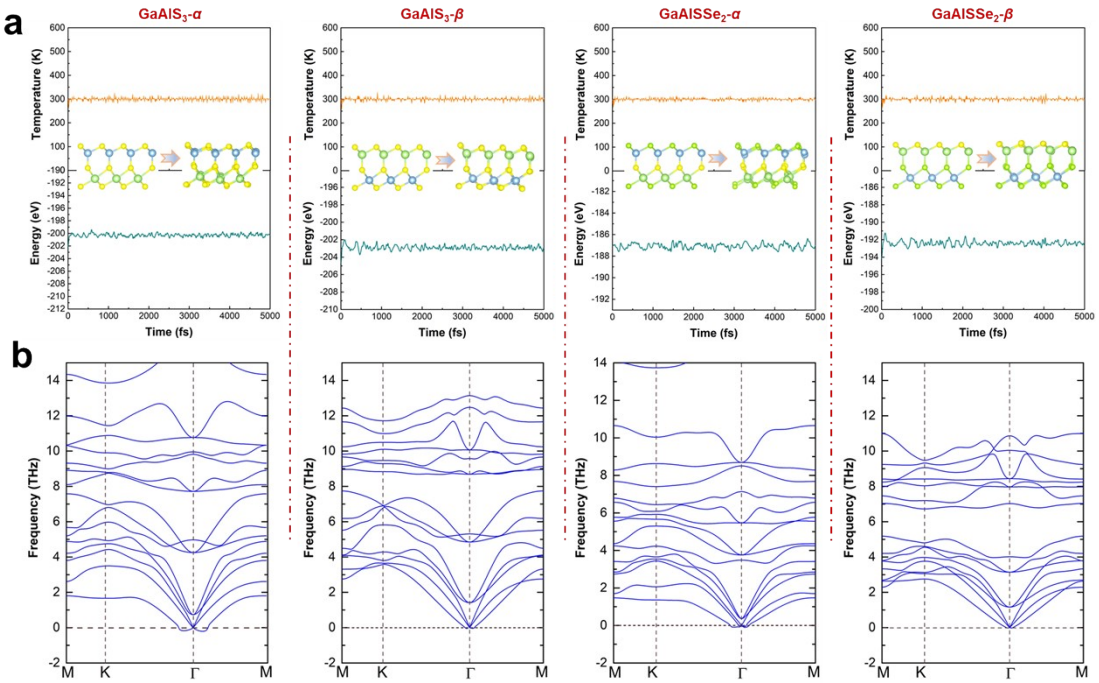

Figure S11. (a) Evolution of total energies (temperatures) from AIMD simulations at 300K and (b) the phonon dispersions for the $GaAlS_3$-α/β and $GaAlSSe_2$-α/β (most stable type) derivatives.

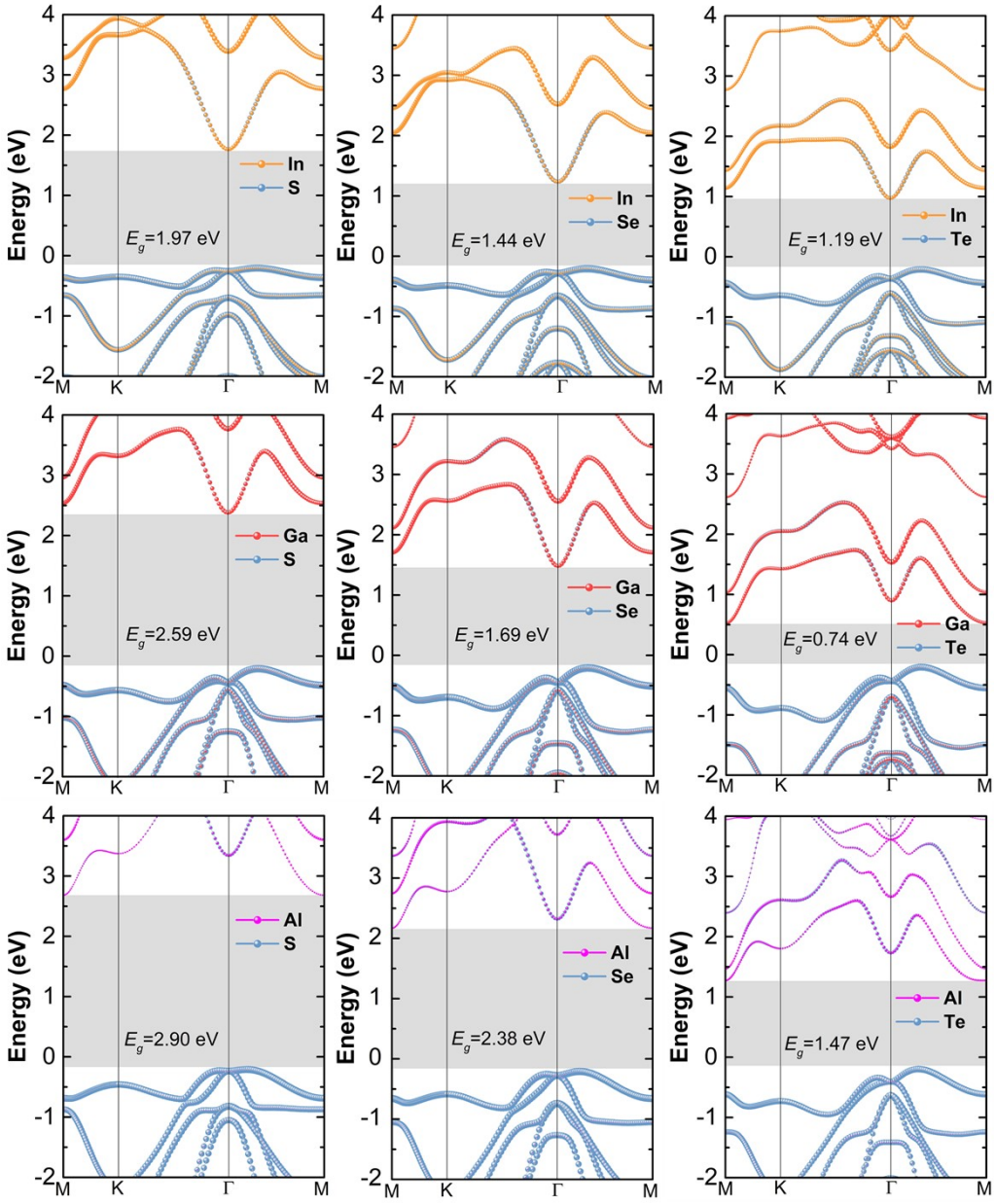

Figure S12 Calculated band structures of the pristine M_2X_3 monolayers (M = In/Ga/Al, X = S/Se/Te) under the HSE06 functional. The Fermi levels are set to 0 eV.

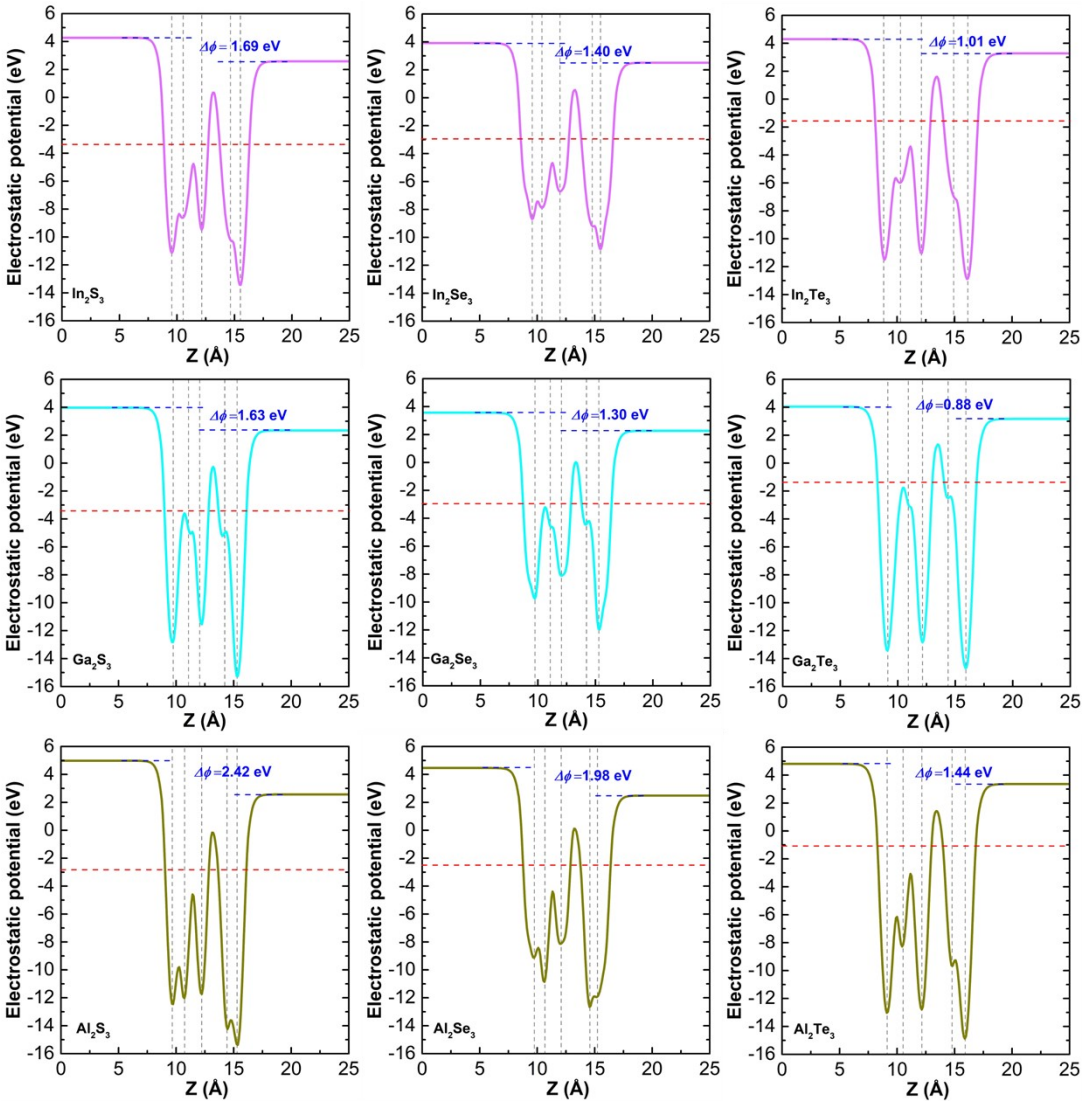

Figure S13 Calculated plane-averaged electrostatic differences of the pristine Group-III trichalcogenide M_2X_3 monolayers (M = In/Ga/Al, X = S/Se/Te) with the HSE06 potential. The red dashed lines represent Fermi levels.

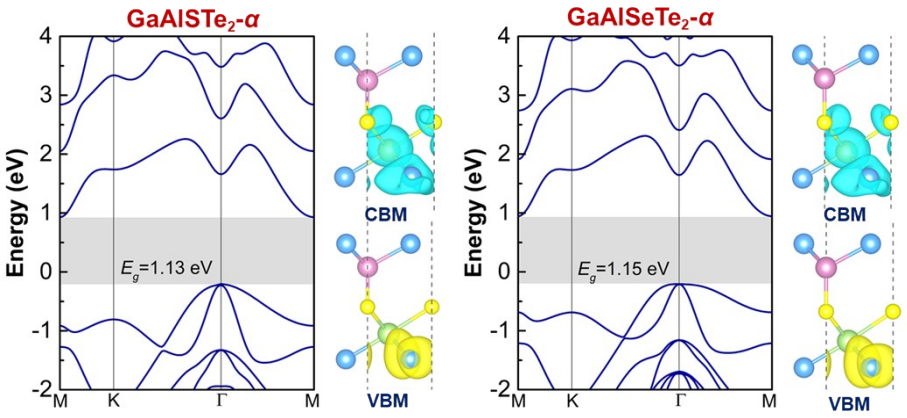

Figure S14 The orbital-projected band structures and partial charge densities of the CBMs and VBMs for the $GaAlSTe_2$-α and $GaAlSeTe_2$-α monolayers.

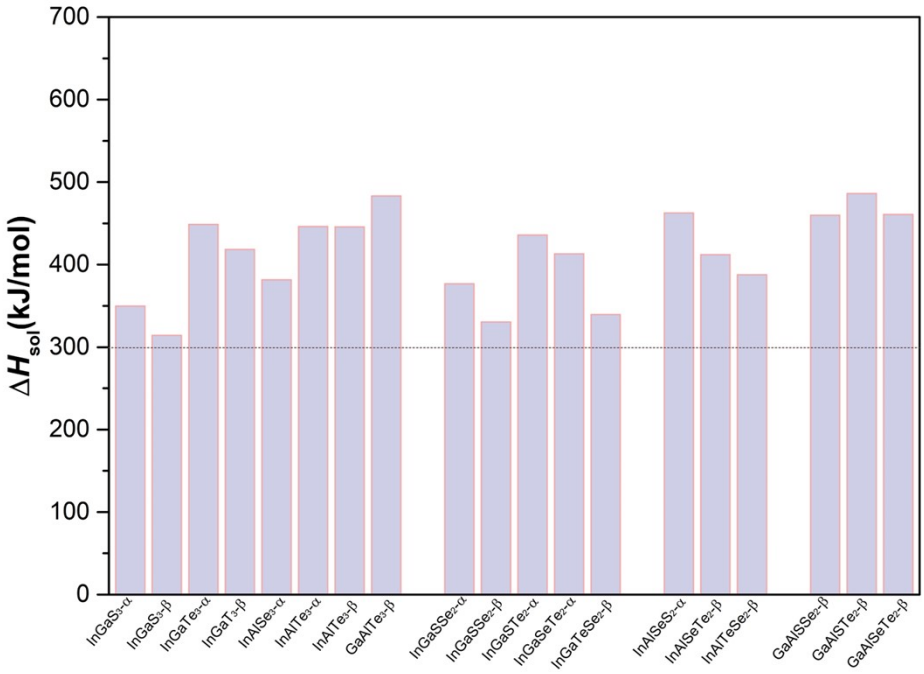

Figure S15 Calculated enthalpy of solvation ΔH_{sol} for the 19 MNX_3 and $MNXY_2$ monolayers (the STH efficiency ≥ 20%). The high ΔH_{sol} suggests that the relevant monolayer is insoluble in water.

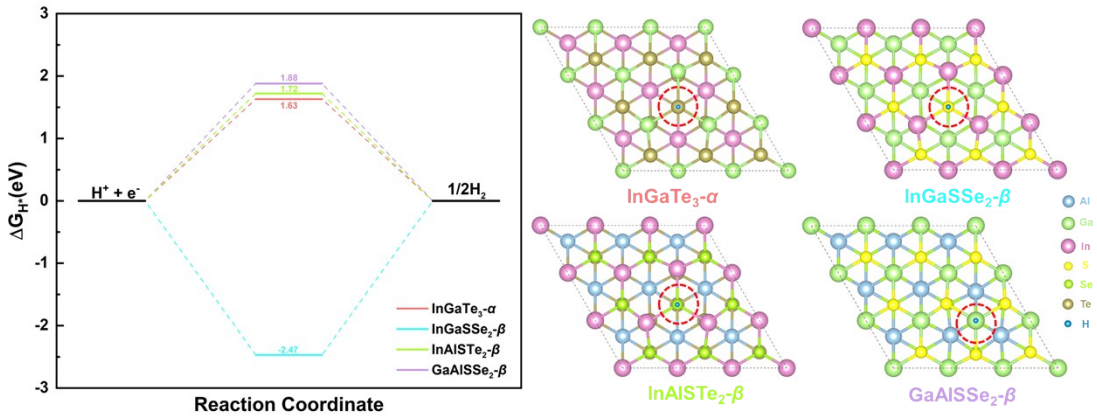

Figure S16 Calculated H adsorption free energy of hydrogen reduction half-reaction in the basal planes of the perfect $InGaTe_3$-α, $GaAlSSe_2$-β, $InGaSSe_2$-β, and $InAlSeTe_2$-β monolayer structures.

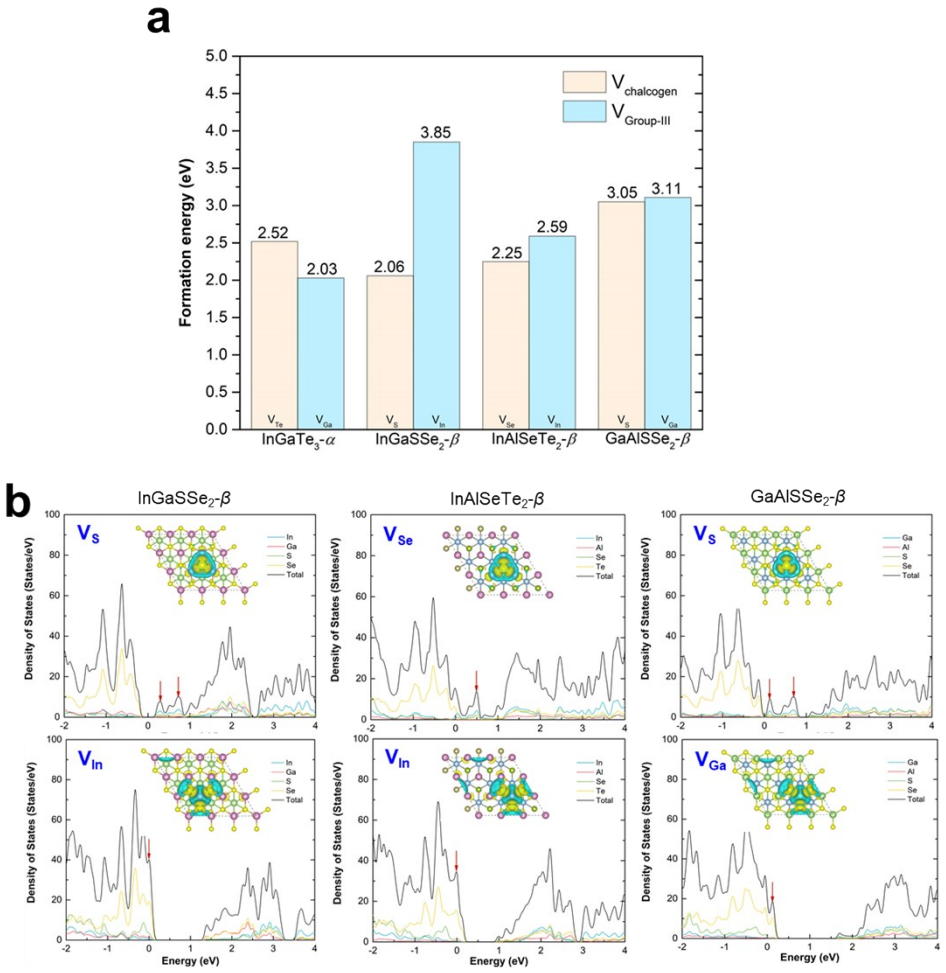

Figure S17. (a) Formation energies of vacancy defects in the $InGaTe_3$-α, $InGaSSe_2$-β, $InAlSeTe_2$-β and $GaAlSSe_2$-β monolayers. (b) The density of states of the $InGaSSe_2$-β, $InAlSeTe_2$-β and $GaAlSSe_2$-β monolayers with vacancy defects. as well as the insets are their charge density differences, here, the orange and blue colors represent electron accumulation and depletion areas.

References

1 C.-F. Fu, J. Sun, Q. Luo, X. Li, W. Hu and J. Yang, *Nano Lett.*, 2018, **18**, 6312–6317.

2 X. Liu, P. Cheng, X. Zhang, T. Shen, J. Liu, J.-C. Ren, S. Li and W. Liu, *J. Mater. Chem. A*, 2021, **9**, 14515.